



# Numerical investigation and feasibility study on MXene/water nanofluid based photovoltaic/thermal system

Sreehari Sreekumar<sup>a,\*</sup>, Nikhilkumar Shah<sup>a</sup>, Jayanta Deb Mondol<sup>a</sup>, Neil Hewitt<sup>a</sup>, Supriya Chakrabarti<sup>b</sup>

<sup>a</sup> Centre for Sustainable Technologies (CST), Belfast School of Architecture and the Built Environment, Ulster University, Newtownabbey BT37 0QB, United Kingdom

<sup>b</sup> Nanotechnology and Integrated Bio-Engineering Centre (NIBEC), Ulster University, Newtownabbey BT37 0QB, United Kingdom



## ARTICLE INFO

### Keywords:

MXene nanofluid  
Nanofluid based PV/T  
CFD  
Enviro-economic analysis

## ABSTRACT

Nanofluid is increasingly adopted in solar collectors as they play a significant role in enhancing the heat transfer process. In this study, a 3D numerical simulation of a nanofluid-based photovoltaic/thermal (N-PV/T) system with MXene nanofluid as heat transfer fluid, was conducted using the finite volume method (FVM). A feasibility analysis was performed on the proposed N-PV/T system. Enviro-economic analysis was also performed from an energy and exergy perspective. The numerical simulation model was validated with experimental and numerical data in the literature and has a minimal error of about 2.75% and 8.9%, respectively. Results indicated that MXene nanofluid of 0.2 wt% achieved a percentage enhancement of 3.5% and 17% electrical efficiency and thermal efficiency, respectively, over water. The 0.2 wt% MXene nanofluid achieved the highest heat transfer coefficient (HTC) of  $261.95 \text{ Wm}^{-2}\text{K}^{-1}$  at a mass flow rate of  $90 \text{ kgh}^{-1}$ . Also, 0.2 wt% nanofluid produced a significant HTC improvement of about 21.42% over water at a flow rate of  $40 \text{ kgh}^{-1}$ . The study showed that MXene nanofluid could effectively reduce the PV surface temperature by 10% compared to water. System size optimization study proved that a 4.5 - 14.5% reduction in the size of PV/T could be achieved with MXene nanofluid. Enviroeconomic analysis showed that the 0.2 wt% nanofluid generated the least emission rate and emission cost according to energy ( $0.42 \text{ kgCO}_2/\text{day}$ , and  $0.028224 \text{ \$/day}$ ) and exergy-based analysis ( $0.48 \text{ kgCO}_2/\text{day}$ , and  $0.032 \text{ \$/day}$ ).

## 1. Introduction

Renewable energy research has produced safer and pollution-free alternative methods to mitigate the excessive utilization of conventional resources to meet the present energy demands. Different energy conversion (photovoltaic (PV), photothermal, and photochemical conversions) methods have been developed to utilize available solar energy resource for various applications (Ahmadi et al., 2021). Photovoltaics is considered to largely contribute to future electricity production. However, the highest achieved PV conversion efficiency is about 30% (Green et al., 2020). Studies show that PV efficiency decreases by 0.4% with each degree rise in temperature (Fouad et al., 2017). Hence, numerous active and passive PV cooling techniques, and hybrid systems have been developed in the past (Kandael et al., 2020). A PV/T collector is a hybrid solar energy conversion device that produces high-grade electricity and low-grade heat as output. A typical PV/T system comprises a PV, an absorber sheet (fixed to the rear end of the PV module), and heat transfer fluid (HTF). The unused thermal energy incident on the top PV surface gets transmitted to the HTF by both conduction and convection modes of heat transfer.

Conventional liquid heat transfer fluids include deionized water, glycol (ethylene glycol, propylene glycol), thermal oils, and ionic liquids (Sreekumar et al., 2022). Numerous studies have evaluated the performance of hybrid PV/T with conventional fluids. Radwan et al. (2020) designed a novel vacuum-based PV/T (VPV/T) system working on the water as HTF. The novel design outperformed the conventional PV/T system at Reynolds number above 60. Salameh et al. (2021) performed a novel 3D simulation of a PV/T system for hot climatic conditions. The  $k-\epsilon$  turbulence model was used for flow simulation. The thermal efficiency of the PV/T system was 60% and 68% at a flow rate of 0.4 and 5.4 L/min, respectively. Conventional HTFs face the disadvantage of poor thermo-physical properties and lack of application-specific property tunability.

In comparison with the numerous conventional HTFs, nanofluids are found to possess exceptional thermal, optical and heat transfer properties (Sreekumar et al., 2020). The conventional working fluids act as a medium for dispersing the nanomaterials to generate nanofluid. A better heat transfer fluid is required to possess higher thermal conductivity, lower viscosity, and high dispersion stability. Research on the efficiency enhancement of PV/T with nanofluids has been on the rise. Significant thermal and electrical performance enhancement is be-

\* Corresponding author:

E-mail address: [Sreekumar-S@ulster.ac.uk](mailto:Sreekumar-S@ulster.ac.uk) (S. Sreekumar).

## Nomenclature

### Parameters

A	Aperture area [m <sup>2</sup> ]
C <sub>p</sub>	Specific heat [J kg <sup>-1</sup> K <sup>-1</sup> ]
E	Exergy [J]
g	Acceleration due to gravity [ms <sup>-2</sup> ]
h	Heat transfer coefficient [Wm <sup>-2</sup> K <sup>-1</sup> ]
I	Solar radiation intensity [Wm <sup>-2</sup> ]
k	Thermal conductivity [Wm <sup>-1</sup> K <sup>-1</sup> ]
ṁ	Mass flow rate [kgs <sup>-1</sup> ]
P <sub>pump</sub>	Pump power [W]
ΔP	Pressure drop [Nm <sup>-2</sup> ]
T	Time [s]
T	Temperature [°C]
ΔT	Instantaneous temperature difference [°C]
Q <sub>sol</sub>	Incident solar energy [W]
Q <sub>u</sub>	Useful heat gain [W]
V	Velocity [ms <sup>-1</sup> ]
y	Penetration depth [m]
Q <sub>nf</sub>	Thermal energy of the nanofluid [KJ]

### Greek Symbol

ρ	Density [kgm <sup>-3</sup> ]
ε	Emissivity of glass
φ	Weight percentage [%]
β	PV cell temperature coefficient
η	Efficiency [%]
μ	Viscosity [kgm <sup>-1</sup> s <sup>-1</sup> ]
α	Thermal diffusivity [m <sup>2</sup> s <sup>-1</sup> ]

### Abbreviations

CFD	Computational fluid dynamics
D	Dimension
EVA	Ethyl vinyl acetate
EG	Ethylene glycol
FVM	Finite volume method
HTC	Heat transfer coefficient
HTF	Heat transfer fluid
MWCNT	Multi-walled carbon nanotube
N-PV/T	Nanofluid based photovoltaic/thermal
PV/T	Photovoltaic/thermal

### Subscript

amb	Ambient
in	Inlet
bf	Base fluid
C	Convection
ele	Electrical
ex	Exergy
f	Fluid
nf	Nanofluid
np	Nanoparticle
out	Outlet
ref	Reference
s	Solid
sol	Solar
th	Thermal
w	Wind
wall	Wall

ing reported with the usage of metal (Rejeb et al., 2016), metal oxide (Shahsavari, 2021), and carbon-based nanofluids (Wahab et al., 2020). Khanjari et al. (2016) performed a numerical analysis and studied the effect of fluid inlet temperature and solar irradiation on an N-PV/T collector. Electrical efficiency was observed to decrease linearly with

fluid inlet temperature and solar irradiation. Nasrin et al. (2018) performed an experimental and numerical analysis of a sheet-and-tube absorber integrated PV/T system with multi-walled carbon nanotube (MWCNT) as a working fluid. Brinkman and Maxwell-Garnet's empirical models were used for defining the nanofluid properties. The thermal and electrical energy efficiencies of the PV/T (with 1% of nanofluid) increased by 114 W and 17 W, respectively, with an increase in solar radiation by 100 Wm<sup>-2</sup>. Compared to water cooling, thermal performance was augmented by around 4% with nanofluid-based cooling. Sangeetha et al. (2020) evaluated the impact of nanofluid usage on the PV temperature reduction, electrical, thermal, and exergy efficiencies. The thermal conductivity values of nanofluids improved with temperature and exhibited enhanced PV surface temperature reduction. In comparison to the conventional PV module, the MWCNT based PV/T collector generated around 60% and 32% enhancement in electrical and overall exergy efficiency, respectively. Eisapour et al. (2020) numerically simulated a wavy tube PV/T system working on a novel microencapsulated PCM nano-slurry in ANSYS Fluent®. The MPCM based PV/T system produced an enhancement in electrical and thermal efficiency by 0.6% and 5.18%, respectively over conventional PV/T.

Apart from metal/metal oxide and carbon, carbide/nitride-based nanofluids, a few novel nanofluids were also developed recently. MXene nanoparticle dispersion was found to enhance the thermal conductivity of base fluid significantly. Studies on MXene nanofluid application as an HTF is comparatively less. Rubbi et al. (2020) conducted a numerical investigation on the performance of a sheet-and-tube PV/T system with a novel MXene nanofluid. The finite element method (FEM) of analysis was conducted with a commercial software package. The thermal conductivity and viscosity of the fluid at different temperatures were calculated experimentally and the results showed that the overall energy efficiency as high as 84% was achieved with novel MXene nanofluid. In comparison with alumina nanofluid, the electrical efficiency and HTC improved by 15.44 and 14.3%, respectively. Samyalingam et al. (2020) performed a numerical simulation of a PV/T collector having a sheet-and-tube arrangement and MXene nanofluid. Olein palm oil was used as the base fluid and the results were compared with Al<sub>2</sub>O<sub>3</sub> water-based nanofluid. The thermophysical properties of nanofluid were analysed and used for numerical simulation of PV/T in COMSOL Multiphysics. The maximum enhancement in thermal conductivity reported was about 68.5% at 0.2 wt% nanofluid. The study reported an enhancement in thermal efficiency and HTC of about 16% and 9%, respectively compared to aluminium oxide nanofluid.

The literature review shows that MXene nanoparticle dispersions significantly enhanced the thermal properties of the base fluid. Moreover, investigation on MXene/water nanofluid as heat transfer fluid in PV/T systems is very rare. To the best of the authors' knowledge, a numerical investigation of MXene based N-PV/T system using FVM has not been conducted to date. The present study numerically investigates the thermal and electrical characteristic performance of a hybrid PV/T collector with MXene/Water nanofluid using ANSYS Fluent® 2020 R2. The study was conducted at different nanofluid concentrations and mass flow rates. Thermal and heat transfer performance of the system was conducted. In addition, an environmental and economic analysis of the N-PV/T system was also carried out based on the energy and exergy perspectives.

## 2. Numerical simulation methodology

### 2.1. Geometric model

In this study, a PV/T system with sheet-and-tube absorber geometry was used for simulation. The study investigates heat transfer enhancement of the system with the usage of MXene nanofluid. To reduce the computational time, only a portion of PV/T with a single tube was considered for analysis (Kazemian et al., 2021b). The physical 3D model of the system was generated in SpaceClaim in ANSYS Fluent® and the com-

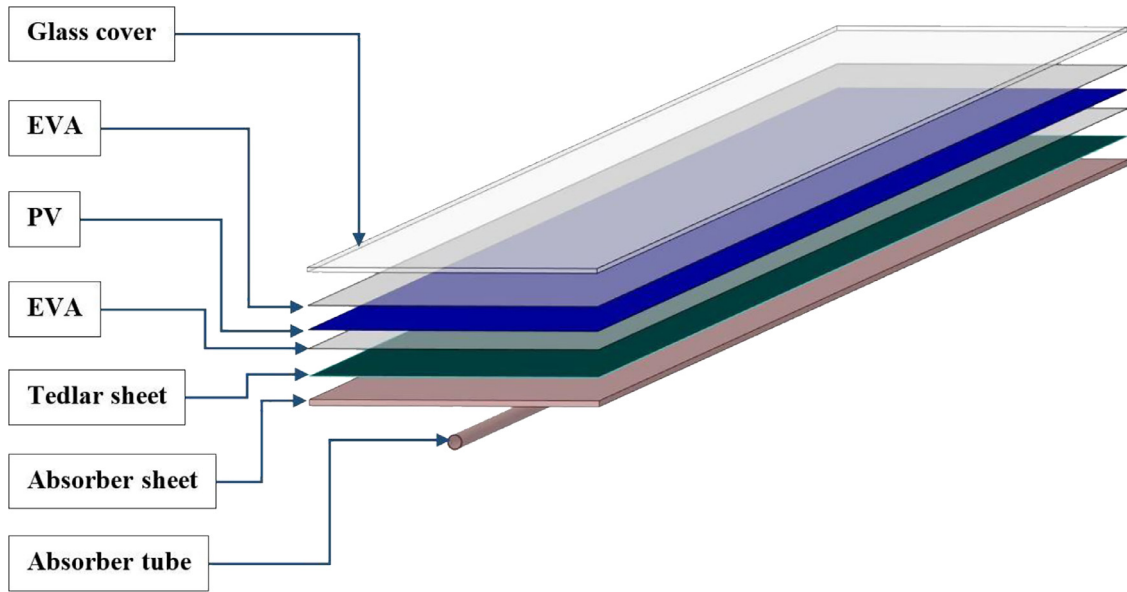


Fig. 1. Exploded view of the proposed PV/T system.

**Table 1**  
PV/T components, dimensions, and material properties used (Kazemian et al., 2021b).

Component (from top to bottom in the geometry)	Dimension (mm)	Thermal conductivity ( $\text{Wm}^{-1}\text{K}^{-1}$ )	Specific heat ( $\text{Jkg}^{-1}\text{K}^{-1}$ )	Density ( $\text{kgm}^{-3}$ )
Glass	$1640 \times 200 \times 3.2$	0.76	830	2200
EVA	$1640 \times 200 \times 0.5$	0.35	2090	960
PV Cell	$1640 \times 200 \times 0.3$	148	700	2330
EVA	$1640 \times 200 \times 0.5$	0.35	2090	960
Tedlar	$1640 \times 200 \times 0.1$	0.2	1250	1200
Absorber sheet	$1640 \times 200 \times 4$	401	385	8960

ponents of the model geometry are arranged in the order (Glass, Ethyl vinyl acetate (EVA), PV, EVA, Tedlar, and Absorber sheet) as shown in Fig. 1. The dimension and material properties of the system components are provided in Table 1. All the material properties and model dimensions were adopted from the literature (Kazemian et al., 2021b). Constant thermal properties were used as the thickness of components are very less, and the variation in results is almost negligible in the temperature range under study (Khanjari et al., 2017).

## 2.2. Governing equations and numeric scheme

The energy equation must be solved along with momentum and conservation equations, to obtain the temperature distribution across the computational domain during simulation. Solving the momentum and conservation equations would provide the information on fluid and flow parameters while solving the energy equation provides the data on heat transfer and temperature of the system components. The basic governing equations that define the computational model is provided below Eqs. (1)-(4) (Arslan et al., 2020).

Continuity equation

$$\frac{\partial \rho_{nf}}{\partial t} + \nabla \cdot (\rho_{nf} \vec{V}_{nf}) = 0 \quad (1)$$

Momentum equation

$$\frac{\partial (\rho_{nf} \vec{V}_{nf})}{\partial t} + \nabla \cdot (\rho_{nf} \vec{V}_{nf} \vec{V}_{nf}) = -\nabla P + \mu_{nf} (\nabla^2 \vec{V}_{nf}) + \rho_{nf} g + S \quad (2)$$

Energy equation for fluid

$$\frac{\partial (\rho_{nf} C_{p,nf} \vec{T}_{nf} \vec{V}_{nf})}{\partial t} = \nabla \cdot (k_{nf} \nabla \vec{T}_{nf}) \quad (3)$$

Energy equation for solid component

$$k_s \nabla^2 (T_s) = 0 \quad (4)$$

Pressure-based FVM was used for solving the proposed numerical model. The thermal and electrical performance of the system would be evaluated at constant operating and environmental parameters. And the efficiency of the system would be measured for each flow rate. Hence, the proposed computational situation could be simulated using a steady-state analysis. The Reynolds number for the flow through the absorber tube was calculated analytically as shown in Table 3. As the Reynolds number calculated for the fluids was much lower than 2300, a laminar flow model was adopted for modelling the fluid flow in the tube (Kanti et al., 2021). Pressure-velocity coupling was performed using the SIMPLE (Semi-Implicit Method for Pressure Linked Equations) algorithm. And second-order upwind scheme was used for discretizing the momentum and energy equations (ANSYS Inc., 2020).

## 2.3. Simulation assumptions and boundary conditions

Assumptions made in the 3D numerical simulation of the N-PV/T system are provided below.

- ∅ Fluid flow was assumed to be laminar, steady, and uniform with developing boundary layer
- ∅ Nanofluid being in thermal equilibrium, a single-phase model was adopted to reduce the computational time and complexity
- ∅ Thermal contact resistance between different solid components was negligible
- ∅ The initial temperature of all solid and fluid components was at the same temperature as the ambient temperature

**Table 2**  
Boundary conditions used for the PV/T system components.

Component	Boundary conditions	
	Top surface	Bottom surface
Glass cover	Conduction, Convection, Radiation $h_w$ : 15.2 W/m <sup>2</sup> K $\epsilon$ : 0.04	Conduction
EVA 1	Conduction	Conduction
PV Cell	Conduction Heat flux: 300 – 1000 W/m <sup>2</sup>	Conduction
EVA 2	Conduction	Conduction
Tedlar	Conduction	Conduction
Absorber sheet	Conduction	Adiabatic to surrounding and Conduction at the tube-absorber interface
Copper tube	Outer surface: Conduction at the tube-absorber interface Adiabatic at surface exposed to ambient	Inner surface: Convection at the tube-fluid interface
Fluid	Inlet temperature: 298 K Mass flow rate: 30–90 kg h <sup>-1</sup>	Convective heat transfer with tube inner surface

- Ø Only glass top surface was having heat transfer to the surrounding by convection and radiation. The bottom and sides of the system domain were assumed to be adiabatic
- Ø The Glass and top EVA layer are assumed to be fully transparent. Hence, the incident solar radiation received on the glass top surface was applied as heat flux to the top of the PV layer
- Ø Heat transfers to all the layers by conduction (from PV surface to Glass, EVA, Tedlar, Absorber sheet, and tube) and convection (from inner tube surface to the fluid)

Boundary conditions used in the model has been detailed in Table 2. The total mass flow rate through the system was divided by the number of absorber tubes and used to define the mass flow rate through a single absorber tube. The pressure was set to atmospheric static pressure at the outlet (Khanjari et al., 2017). The average area-weighted total pressure and temperature at the tube end sections were calculated to find the pressure drop and temperature difference across the length. The boundary condition between a surface and fluid was defined as a ‘no slip’ condition. Wall heat flux was defined as zero for insulation (edges of all layers and bottom surface of absorber sheet) (Rubbi et al., 2020). The emissivity of glass ( $\epsilon$ ) was taken to be 0.04 (Kazemian et al., 2021a). Convective heat transfer ( $h_w$ ) (or heat loss) coefficient due to wind on the glass top surface was calculated using Eqs. (5) and ((6) (Kazemian et al., 2021a). The wind velocity ( $V_w$ ) over the PV/T surface was assumed to be below 5 m/s.

$$h_w = 5.7 + 3.8V_w \text{ for } V_w < 5 \text{ m/s} \quad (5)$$

$$h_w = 6.47 + V_w^{0.78} \text{ for } V_w > 5 \text{ m/s} \quad (6)$$

#### 2.4. Nanofluid modelling

Nanofluid simulation using a single-phase model was adopted as it provides the same results with negligible variation as a mixture model with almost reduced computation complexity (Khanjari et al., 2017). MXene nanofluid of varying concentrations (0.01, 0.1, and 0.2 wt%) was selected for analysis. The upper limit of MXene nanofluid concentration was selected from literature based on the optimum concentration that generates better thermophysical property improvement with a minimum viscosity enhancement (Mahesh et al., 2016; Parashar et al., 2021). Eq. (7) shows the relation between amount of nanomaterial ( $m_{np}$ ), and mass of base fluid ( $m_{bf}$ ) required to develop a nanofluid at a specific concentration ( $\phi_{np}$ ). The effective density, thermal conductivity, specific heat, and viscosity of nanofluids could be calculated using already established relations based on nanofluid concentration (Salari et al., 2020). Models by Pak and Cho (Equation ((8)), Xuan and Roetzel (Eq. (9)), Brinkman (Eq. (10)), Hamilton and Crosser (Eq. (11))

are used for density, specific heat, viscosity, and thermal conductivity calculations, respectively (Pordanjani et al., 2021). Hamilton and Crosser’s model was found to be predicting the thermal conductivity of nanofluid containing dispersions of nanosheet geometry similar to MXene nanosheet (Hussien et al., 2017). These equations are used to find the effective properties of nanofluids based on the base fluid properties and nanoparticle concentration. The thermal conductivity and viscosity variation of MXene nanofluid with particle concentration is depicted in Fig. 2.

$$\phi_{np} = \frac{m_{np}}{m_{np} + m_{bf}} \quad (7)$$

$$\rho_{nf} = \phi_{np}\rho_{np} + (1 - \phi_{np})\rho_{bf} \quad (8)$$

$$C_{p, nf} = \frac{\phi_{np}\rho_{np}C_{p,np} + (1 - \phi_{np})\rho_{bf}C_{p,bf}}{\rho_{nf}} \quad (9)$$

$$\mu_{c,p, nf} = \frac{\mu_{bf}}{(1 - \phi_{np})^{2.5}} \quad (10)$$

$$K_{nf} = K_{bf} \frac{(K_{np} + 2K_{bf}) - 2\phi_{np}(K_{bf} - K_{np})}{(K_{np} + 2K_{bf}) + \phi_{np}(K_{bf} - K_{np})} \quad (11)$$

A drawback with the present model is the inability to model the stability of nanofluid. Nanoparticles are subjected to particle agglomeration and results in sedimentation, thus degrading the thermophysical properties. However, there is no existing model that could address the problem. MXene nanofluid was also selected as it possesses comparatively higher colloidal stability over conventional nanofluids (Bao et al., 2021). Hence, the effect of nanofluid stability on the results is minimal.

#### 2.5. Thermodynamic and heat transfer analysis

##### 2.5.1. Heat transfer analysis

The surface average HTC ( $h_c$ ) was calculated directly from the post-processing phase with the generated data (wall heat flux, surface temperature, and bulk fluid temperature) from the simulation, for each case of study. The equation used for HTC calculation is provided below:

$$h_c = \frac{m_f \times C_{p,f} (T_{out} - T_{in})}{A(T_{wall} - T_f)} \quad (12)$$

Pressure drop across the tube was calculated using Eq. (13) from the post-processing step. Pump power can be directly calculated from mass flow rate, nanofluid density, and pressure drop across the tube (Mashhadian et al., 2021) as shown in Eq. (14).

$$\Delta P = P_{in} - P_{out} \quad (13)$$

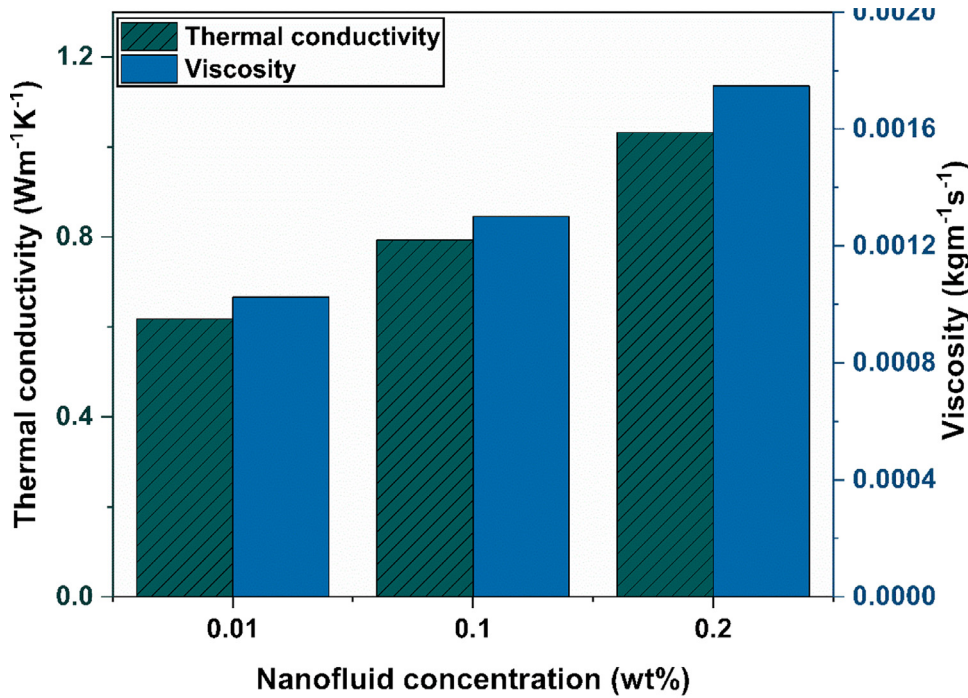


Fig. 2. Thermal conductivity and viscosity variation with the concentration of MXene nanofluid.

$$W_{pump} = \frac{\dot{m}}{\rho_{nf}} \times \Delta P \quad (14)$$

### 2.5.2. Energy efficiency analysis

The thermal efficiency of the system is calculated using Eq. (15). In this equation, the mass flow rate and specific heat of nanofluid, incident solar radiation, aperture area, and inlet temperatures are known. The useful thermal energy ( $Q_u$ ) produced from the solar irradiation by heat transfer from the PV module is calculated using Eq. (16). The outlet temperature will be calculated after solving the energy equation during numerical simulation.

$$\eta_{th} = \frac{Q_u}{A \times I} \quad (15)$$

$$Q_u = m_f \times C_{p,f} (T_{out} - T_{in}) \quad (16)$$

The electrical efficiency ( $\eta_{th}$ ) of the PV/T system would be varying with the PV surface temperature and be calculated using Eq. (17). The parameters required for the calculations are reference efficiency, temperature coefficient, and the cell temperatures at a particular time and standard test condition ( $\eta_{ref}$ ,  $\beta$ ,  $T_{cell}$ , and  $T_{ref}$ , respectively) (Khanjari et al., 2017). The reference temperature and efficiency of the PV are known. Numerical simulation will provide the value of cell temperature at each point during the operational time. Cell temperature coefficient varies for each PV module used (0.0027 for polycrystalline PV (Aste et al., 2012), the monocrystalline cell is about 0.0045 (Kazemian et al., 2021a)).

$$\eta_{ele} = \eta_{ref} \times (1 - \beta(T_{cell} - T_{ref})) \quad (17)$$

### 2.5.3. Exergy efficiency analysis

The quality of the energy and irreversibilities during the PV/T performance were taken into consideration in the exergy analysis. Thermal exergy efficiency was calculated to find the exergy destruction associated with the system. Input exergy entering the domain was the exergy from solar radiation and fluid inflow. Exergy exiting the system was contributed by heat loss from PV/T surface to surrounding and exergy due to fluid outflow. The net exergy balance calculation was conducted as

shown in Eq. (18). Eq. (19) was used to calculate the exergy from solar radiation. The temperature of the sun was taken to be 5774 K. The net thermal exergy gain by the fluid was obtained using Eq. (20). The thermal exergy efficiency of the PV/T system was obtained by substituting Eqs. (19) and (20) in Eq. (21).

$$E_{ex,in} = E_{ex,out} + E_{ex,loss} \quad (18)$$

$$E_{ex,sol} = IA \times \left(1 - \frac{T_{amb}}{T_{sun}}\right) \quad (19)$$

$$E_{ex,th} = Q_u - \dot{m}C_p T_{amb} \ln\left(\frac{T_{out}}{T_{in}}\right) \quad (20)$$

$$\eta_{ex,th} = \frac{E_{ex,th}}{E_{ex,sol}} = \frac{Q_u - \dot{m}C_p T_{amb} \ln\left(\frac{T_{out}}{T_{in}}\right)}{IA \times \left(1 - \frac{T_{amb}}{T_{sun}}\right)} \quad (21)$$

The electrical exergy of the PV/T system is the high-grade electrical energy output generated by the PV/T module. The electrical exergy was calculated by dividing the electrical exergy of the system by incident exergy, as shown in Eq. (23) (Shahsavari, 2021).

$$E_{ex,ele} = IA \times \eta_{PV} \quad (22)$$

$$\eta_{ex,ele} = \frac{E_{ex,ele}}{E_{ex,sol}} = \frac{IA \times \eta_{PV}}{IA \times \left(1 - \frac{T_{amb}}{T_{sun}}\right)} \quad (23)$$

### 2.6. Meshing and grid independence test

Poly-hexacore shape with mosaic meshing technique was used for meshing the geometric model, as shown in Fig. 3. The mesh quality was also found to be superior and produced same results with a minimum number of elements in comparison to the tetrahedral meshing. An extensive grid-independence test was performed along all the dimensions using local sizing controls to analyse the component that was more sensitive to number to grid elements. The element size adopted for the meshing was in the range of 0.0015 to 0.005 m. The number of elements of the domain was varied from 1.5 to  $5 \times 10^5$ . As seen from Fig. 3, the final

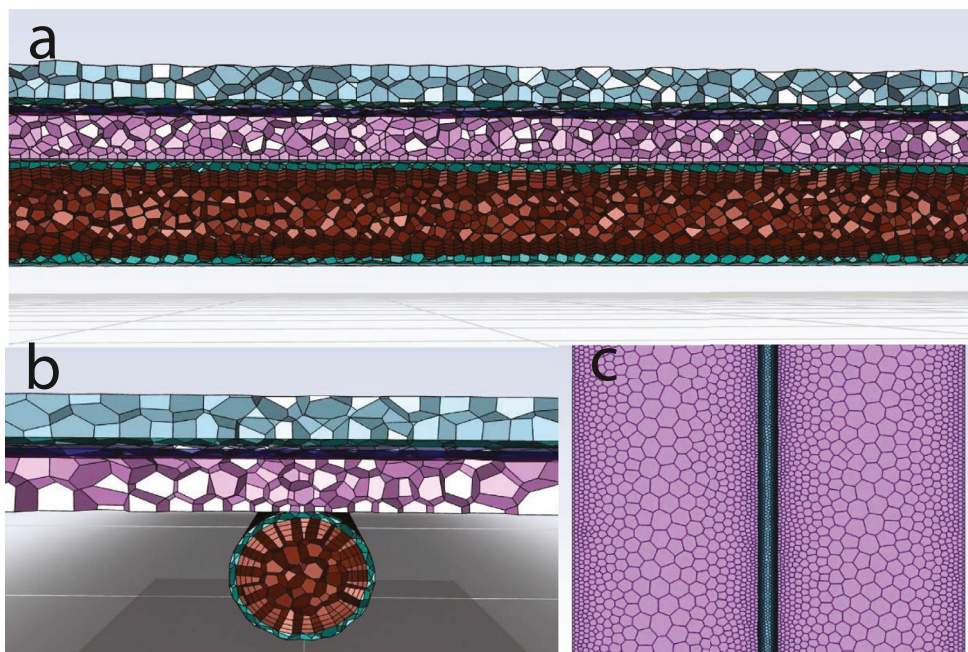


Fig. 3. Mesh alignment (a) along the length (b) across the width and (c) over the PV/T bottom surface.

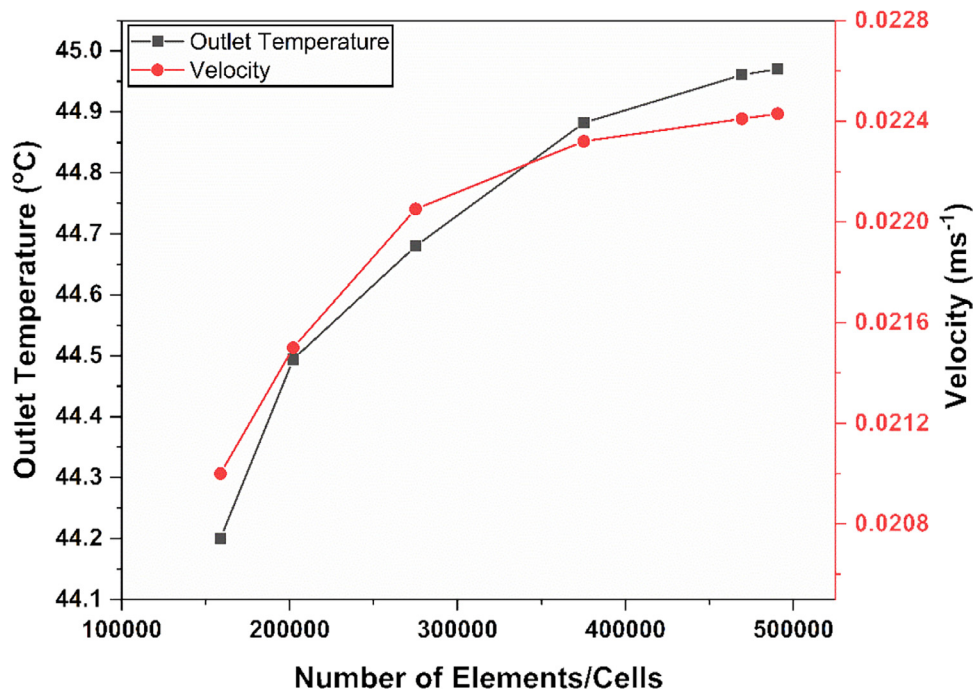


Fig. 4. Grid independence test performed on the model at base conditions.

mesh consists of finer mesh in the fluid and tube regions. For each case, steady-state simulation was performed on the system under the same input parameters values for solar radiation, flow rate, and inlet temperature ( $470 \text{ Wm}^{-2}$ ,  $0.00136 \text{ kgs}^{-1}$ , and  $305 \text{ K}$ , respectively) were used for the analysis. Negligible variation in outlet temperature and outlet velocity was observed for each case. As observed from Fig. 4, only a  $0.7 \text{ }^\circ\text{C}$  change in the outlet temperature was present during grid-sensitive analysis. Also, a minute variation in outlet temperature by around  $0.5\%$  was noticed while changing the number of elements from  $3.7$  to  $4.9 \times 10^5$ .

### 2.7. Numerical model validation

The present model was validated with the experimental data for Selmi et al. (2008). The inlet temperature ( $32\text{--}46 \text{ }^\circ\text{C}$ ), solar radiation ( $470\text{--}542 \text{ Wm}^{-2}$ ), and mass flow rate ( $0.00136 \text{ kgs}^{-1}$ ) values from the

study were adopted as operating conditions for simulating the proposed PV/T model. The dimensions of the 3D PV/T model were almost the same as that of the literature. The Fig. 5 shows that the fluid outlet temperature predicted by the numerical model agrees with the experimental data. During the error analysis, it was observed that the relative variation of results with that of experimental (Selmi et al., 2008) study was only  $8.97\%$ .

## 3. Results and discussion

### 3.1. Numerical simulation

A numerical investigation was conducted initially to study the effect of different working fluids (MXene/Water, Water, and EG) on the thermal performance of the system. The study was performed by varying

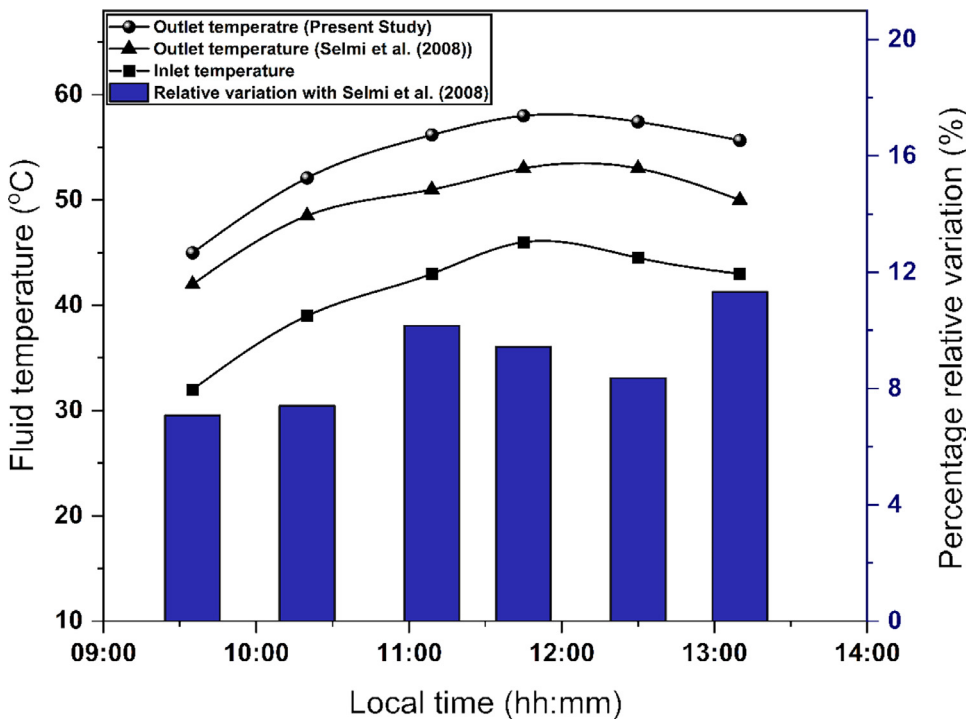


Fig. 5. Validation of the proposed model with Selmi et al. (2008).

mass flow rates (ranging from 30–90  $\text{kg h}^{-1}$ ), while all other operating parameters (including inlet temperature, and solar radiation) were kept constant. The simulation data were analysed to evaluate the better base fluid to be used as heat fluid in the PV/T system. System performance comparisons with water and ethylene glycol working fluids were conducted. Four parameters (namely, thermal efficiency, electrical efficiency, HTC, and pressure drop) were used for the evaluation.

### 3.1.1. Thermal efficiency

Water was found to be a better base fluid in comparison to EG as the system generated higher thermal and electrical efficiency with minimum pressure drop. Higher thermal conductivity and low viscosity of water facilitate a higher heat transfer rate compared to EG (Sreedhar et al., 2020) and hence selected as base fluid. MXene/water nanofluid of three different mass fractions (0.01, 0.1, and 0.2 wt%) was considered for further analysis. As observed in Fig. 6 (a), the mass flow rate of the working fluid was found to be linearly influencing the thermal efficiency of the system with maximum thermal efficiency at 90  $\text{kg h}^{-1}$ . The outlet temperature of the fluid which determines the thermal efficiency is dependent on the heat transfer rate in the tube. With the increase in flow rate, the heat transfer rate from the tube surface to the fluid would be enhanced considerably (Kazemian et al., 2021b; Kianifard et al., 2020). This has contributed to improvement in HTC in the tube as seen in Fig. 8 (a). Also, an increase in flow rate reduces the heat loss from the system as the surface temperature achieved by the PV/T surface exposed to the ambient would be comparatively small. The highest thermal efficiency of 67.49% was reported with 0.2 wt% MXene nanofluid. Around 63% and 60.4% thermal efficiency were shown by MXene nanofluids of 0.1 and 0.01 wt%, respectively. Increasing the mass flow rate of 0.2 wt% nanofluid by 60  $\text{kg h}^{-1}$  produced about a 21% increase in the thermal efficiency of the system. As observed from Fig. 6 (b), MXene nanofluid (0.2 wt%) based system reported the highest percentage enhancement in thermal efficiency by 17% over the water-based system. Correspondingly, the highest percentage improvement by 0.1 wt% and 0.01 wt% over water were 9.1% and 6.3%, respectively.

### 3.1.2. Electrical efficiency

Variation in electrical efficiency of the system with working fluids at various mass flow rates is shown in Fig. 7. The PV efficiency is inversely related to the module surface temperature as seen in Eq. (17). An increase in mass flow rate reduces the PV temperature and thereby improves the electrical efficiency of PV/T (Shahsavari, 2021). As observed, the PV efficiency improvement was linear and marginal. The highest electrical efficiency of 15.94% was obtained for 0.2 wt% nanofluid. The nanofluid exhibited the highest enhancement in electrical efficiency of the system compared to water by about 3.55% at a flow rate of 30  $\text{kg h}^{-1}$ . On varying the flow rate from 30  $\text{kg h}^{-1}$  to 90  $\text{kg h}^{-1}$ , the percentage change in electrical efficiency for 0.01, 0.1, and 0.2 wt% nanofluids was found to be about 4.08, 4.16, and 4.23%, respectively.

### 3.1.3. Surface heat transfer coefficient

The outlet temperature and surface temperature were observed to decrease with an increase in the mass flow rate. The surface temperature profile was found to be almost parallel with the fluid outlet temperature with an increasing flow rate. As the flow rate increases, the velocity increases and consequently increases the HTC. The convective heat transfer from the system is maximum at higher flow rates. At lower flow rates, velocity is lower, and the fluid takes more time to cover the absorber length. Consequently, the HTC of the inner tube decreases and hence decreased heat transfer. The HTC of the inner tube surface with each working fluid is shown in Fig. 8 (a). As the flow rate increases, the HTC was found to increase. HTC of 0.2 wt% nanofluid increased from 177.209  $\text{W m}^{-2}\text{K}^{-1}$  at a flow rate of 30  $\text{kg h}^{-1}$  to about 262  $\text{W m}^{-2}\text{K}^{-1}$  at 90  $\text{kg h}^{-1}$  provided all other operating conditions are kept constant. HTC normally increases steadily with an increase in nanofluid concentration (Ekiciler et al., 2020; Gupta et al., 2020). Multiple factors govern the HTC of a fluid flow. Viscous effects and boundary layer development tend to reduce the heat transfer coefficient. However, the high thermal diffusivity of nanofluid was observed to have overcome the viscous effects and produced an enhancement in HTC over less viscous base fluids. About 18.5% enhancement in surface HTC value (at 90  $\text{kg h}^{-1}$ ) was

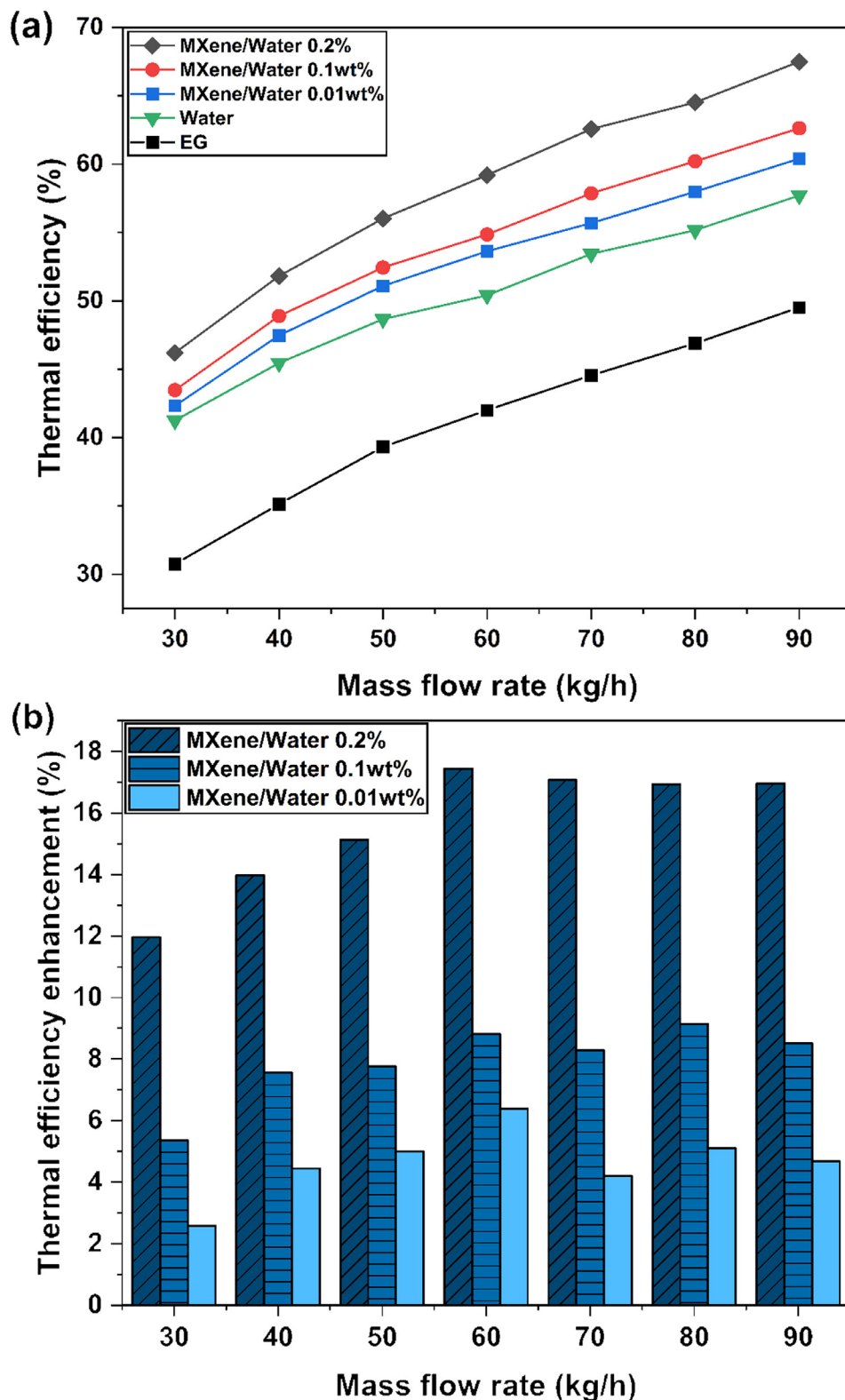


Fig. 6. (a) Effect of mass flow rate on the thermal efficiency of the system (b) Percentage enhancement in thermal efficiency of nanofluid based system over water.

observed while increasing the concentration of nanofluid from 0.01 to 0.2 wt%. Hence the heat transfer rate was found to increase linearly with an increase in the flow rate and mass fraction of nanofluid. The percentage relative enhancement of HTC with nanofluid flow over water is shown in Fig. 8 (b). MXene nanofluid (0.2 wt%) achieved the highest enhancement at a mass flow rate of 90 kg h<sup>-1</sup> with a significant improvement of 21.42% over water.

### 3.1.4. Pressure drop

Pressure drop generated during the flow of base fluids and nanofluids at different mass flow rates were calculated and depicted in Fig. 9. Viscous fluids offer higher resistance to the flow and contribute to pressure loss (Karaaslan and Menlik, 2021). As ethylene glycol is having higher viscosity compared to water, the pressure drop was observed to be increasing, from 217 to 676 Pa, with an increase in mass flow rate from

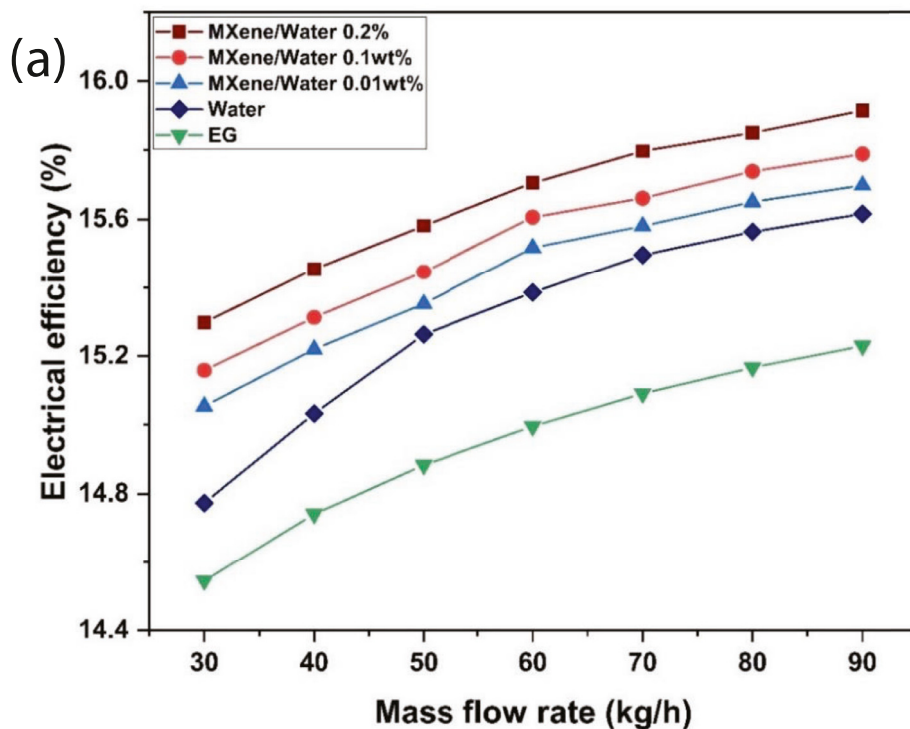
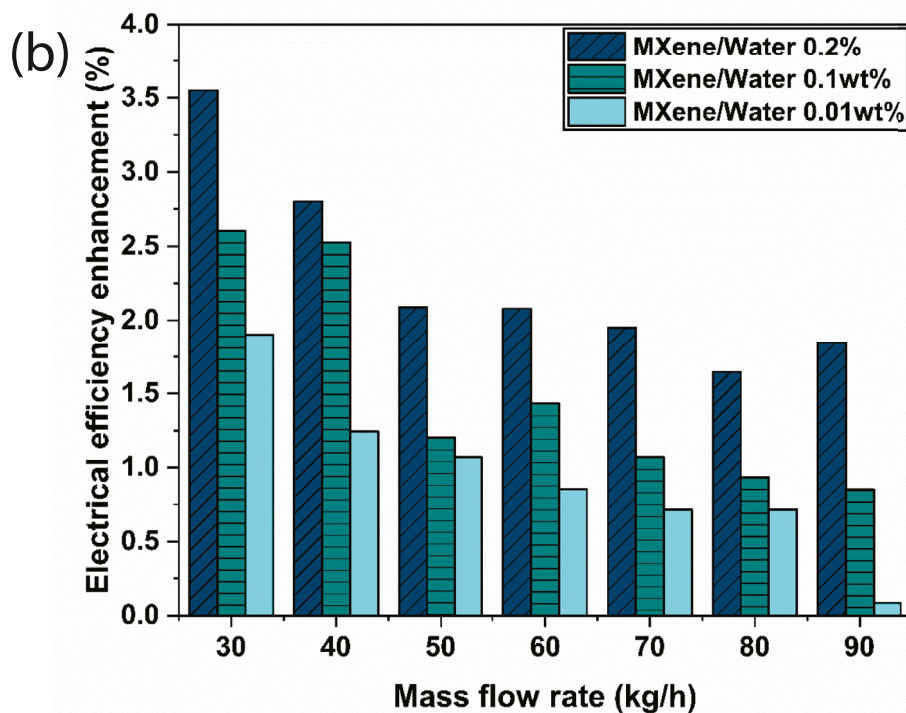


Fig. 7. (a) Effect of mass flow rate on electrical efficiency of the system (b) Percentage enhancement of electrical efficiency of nanofluid based system over water.



30 to 90 kg h<sup>-1</sup>. Hence, water was only considered to be an option for further analysis as a base fluid. As, the viscosity of nanofluid is directly dependent on particle concentration, pressure drop was observed to be highest for 0.2 wt% nanofluid. Also, the pressure drop increased with fluid mass flow rate. MXene/water nanofluid with 0.01 wt% showed an average increase in pressure drop by about 14% over water. However, for the case of 0.2 wt% nanofluid, the pressure drop increased by about 88% over water. Even though the percentage enhancement was higher

compared to water, the corresponding pumping power was negligible and much below that of EG. For the present case of MXene nanofluid, the heat transfer enhancement achieved was much higher compared to the pressure drop penalty.

### 3.1.5. Temperature distribution

Outlet temperature for each nanofluid and water was visualized using a 2D cross-sectional temperature contour plot of fluid volume (see

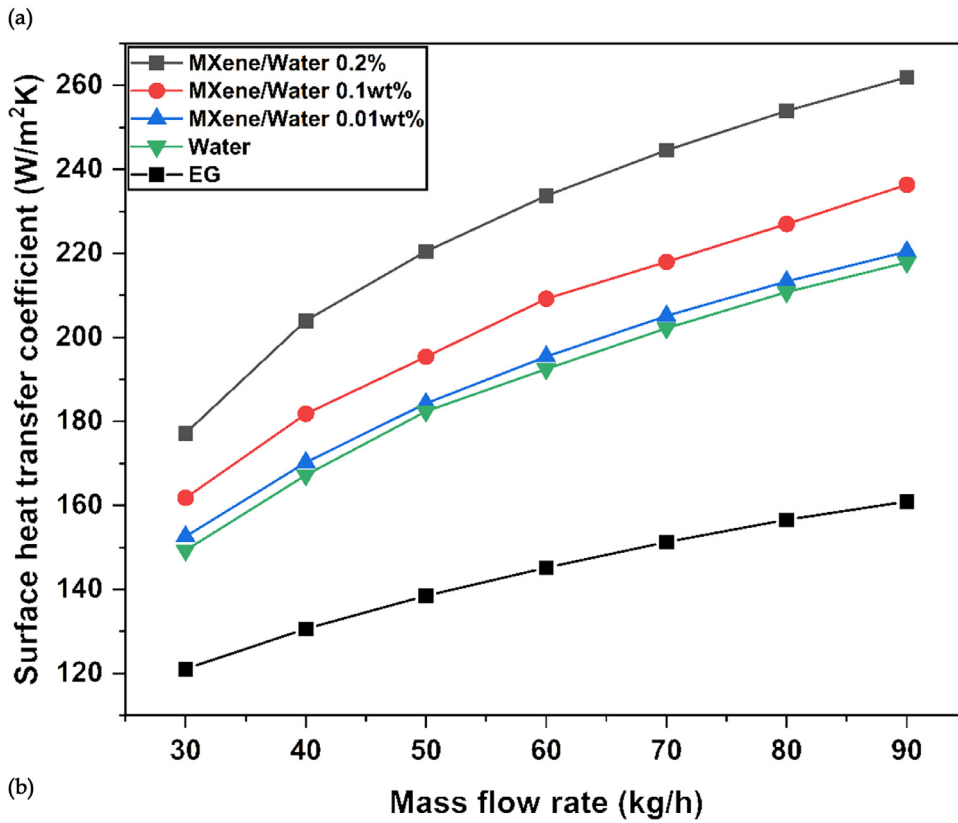


Fig. 8. Effect of nanofluid mass flow rate on surface HTC of the system and (b) Percentage relative enhancement of HTC with nanofluid over water.

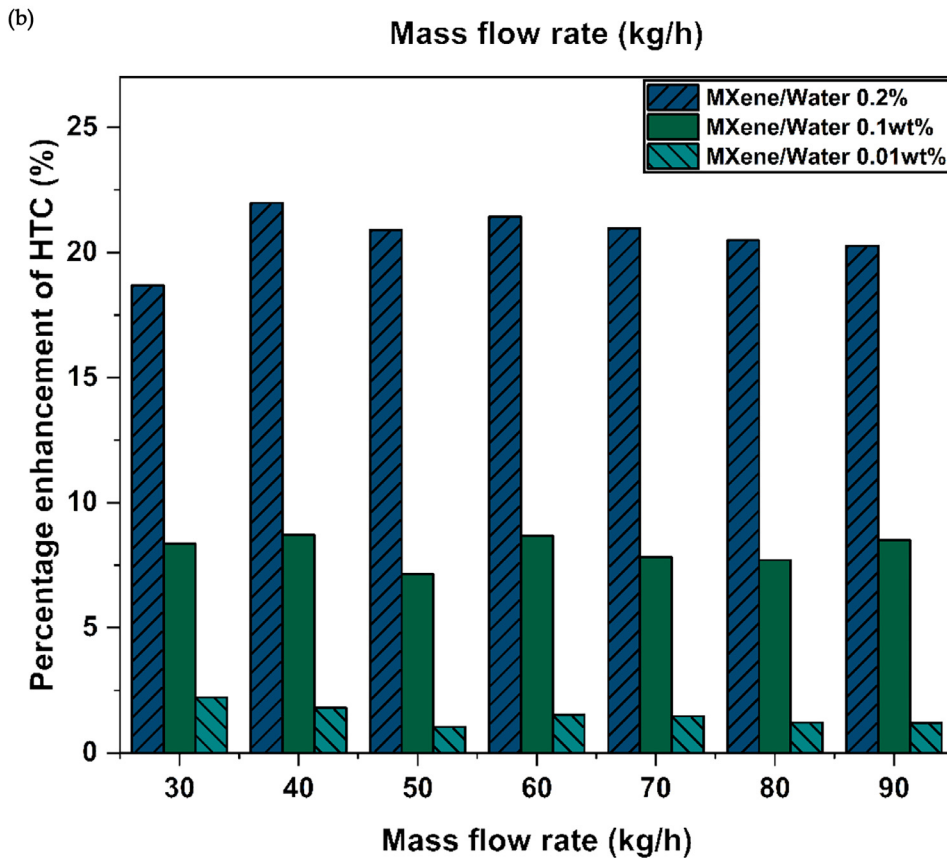


Fig. 10). Analysis was performed with the system operating at base conditions (solar radiation ( $800\text{Wm}^{-2}$ ), inlet temperature ( $25^\circ\text{C}$ ), and ambient temperature ( $25^\circ\text{C}$ )). Area weighted average fluid temperature at the outlet was used for post-data analysis. A higher temperature was observed for the fluid volume portion at the top, where the tube is in

contact with the absorber sheet. A slight temperature gradient was observed between the top and center of fluid volume as flow is laminar and no external turbulence is created. MXene nanofluid of 0.2 wt% produced the highest outlet temperature compared to other fluids as thermal transport in the fluid was increased with concentration. This behaviour could

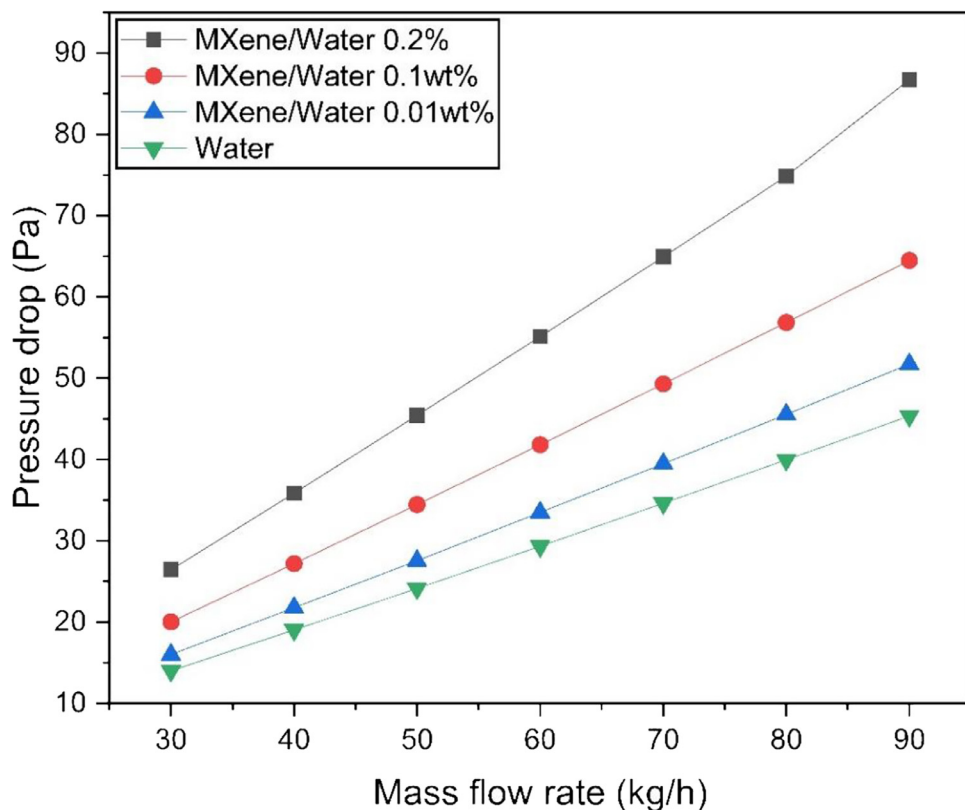


Fig. 9. Effect of nanofluid mass flow rate on pressure drop developed in tube.

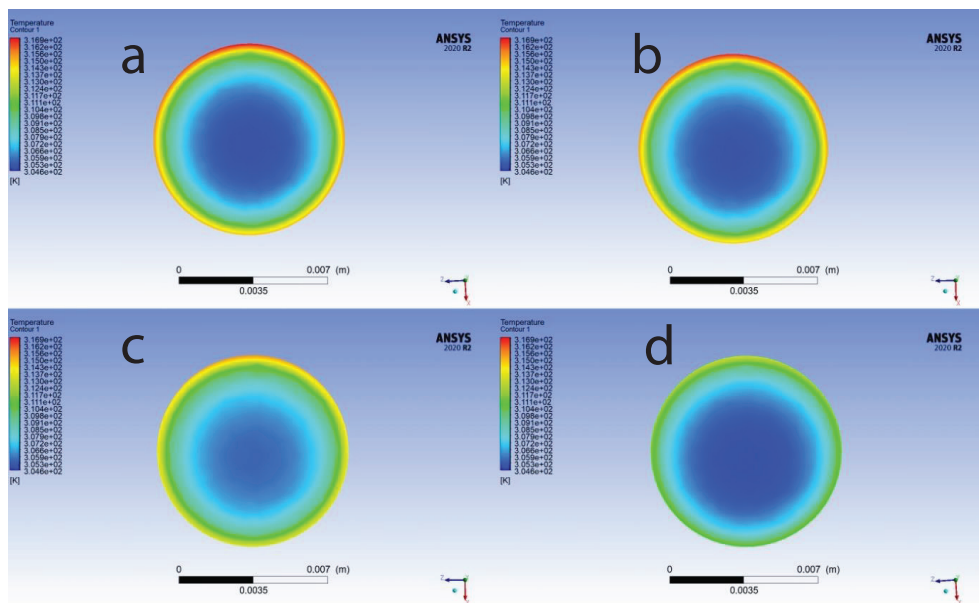


Fig. 10. Fluid cross-sectional temperature distribution at outlet for (a) 0.2 wt% MXene (b) 0.1 wt% MXene (c) 0.01 wt% MXene and (d) water.

be attributed to the thermal diffusivity of the nanofluid. As observed in Table 3, thermal diffusivity increased with nanofluid concentration due to enhancement in thermal conductivity. Hence, Fig. 10 shows that 0.2 wt% nanofluid has the highest thermal diffusivity in comparison to other fluids. Streamlines during the tube flow of 0.2 wt% nanofluid at inlet and outlet sections are depicted in Fig. 11. Due to boundary layer development as observed in the figure, the viscous effects decrease towards the centre of the tube, resulting in an increase in velocity and thereby reduced thermal diffusion.

The corresponding PV surface temperatures for the HTFs could be observed in Fig. 12. The module surface temperature was calculated for

various flow rates (30, 50, 70, and 90 kg h<sup>-1</sup>) at a constant solar radiation intensity of 800 W m<sup>-2</sup>. The 0.1 wt% MXene nanofluid was taken for studying the effect of mass flow rate on PV surface temperature. As interpreted from the figure, the surface temperature is considerably reduced with increased mass flow rate, by approximately 10 °C. Enhancement in HTC with mass low rate has effectively contributed to the reduction of PV surface temperature.

Fig. 13, shows the PV surface temperature reduction achieved with each working fluid at corresponding mass flow rates. The PV surface temperature was noted to be decreasing with an increase in nanofluid concentration and mass flow rate. Around 10% reduction in PV surface

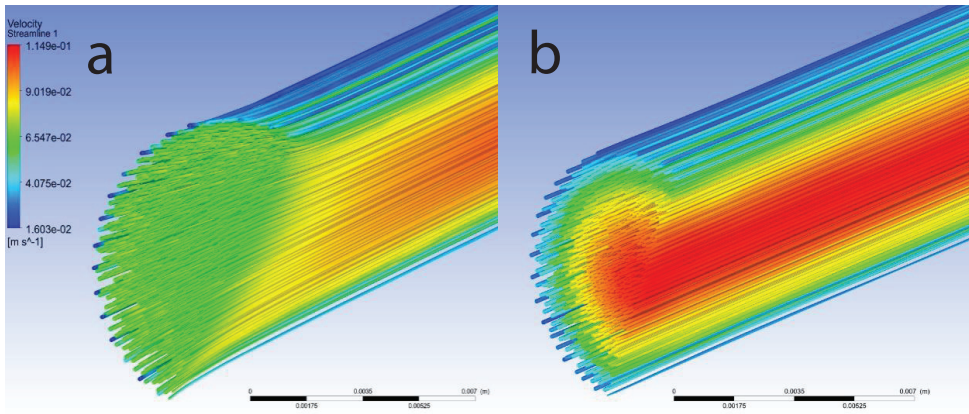


Fig. 11. Streamlines during nanofluid (0.2 wt%) flow through the tube at (a) inlet and (b) outlet.

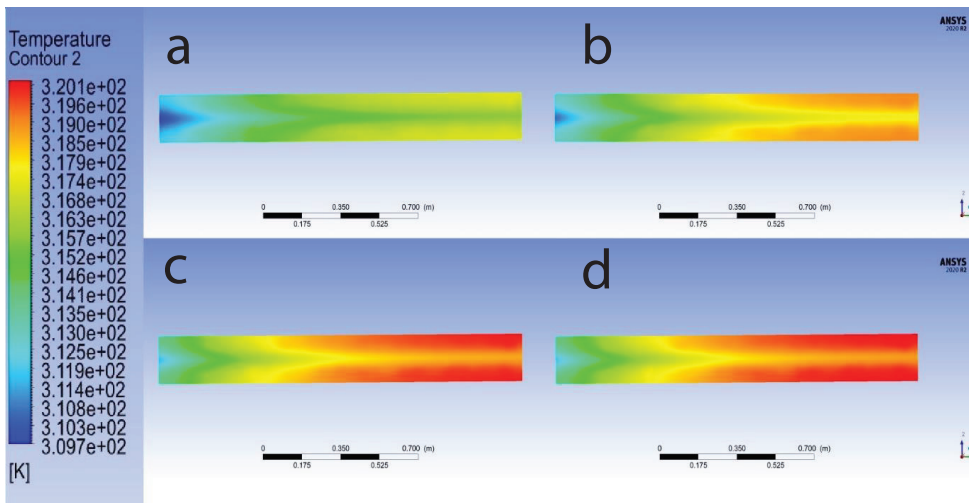


Fig. 12. Surface temperature of PV module with (a) 0.2 wt% MXene nanofluid (b) 0.1 wt% MXene nanofluid (c) 0.01 wt% MXene nanofluid and (d) water.

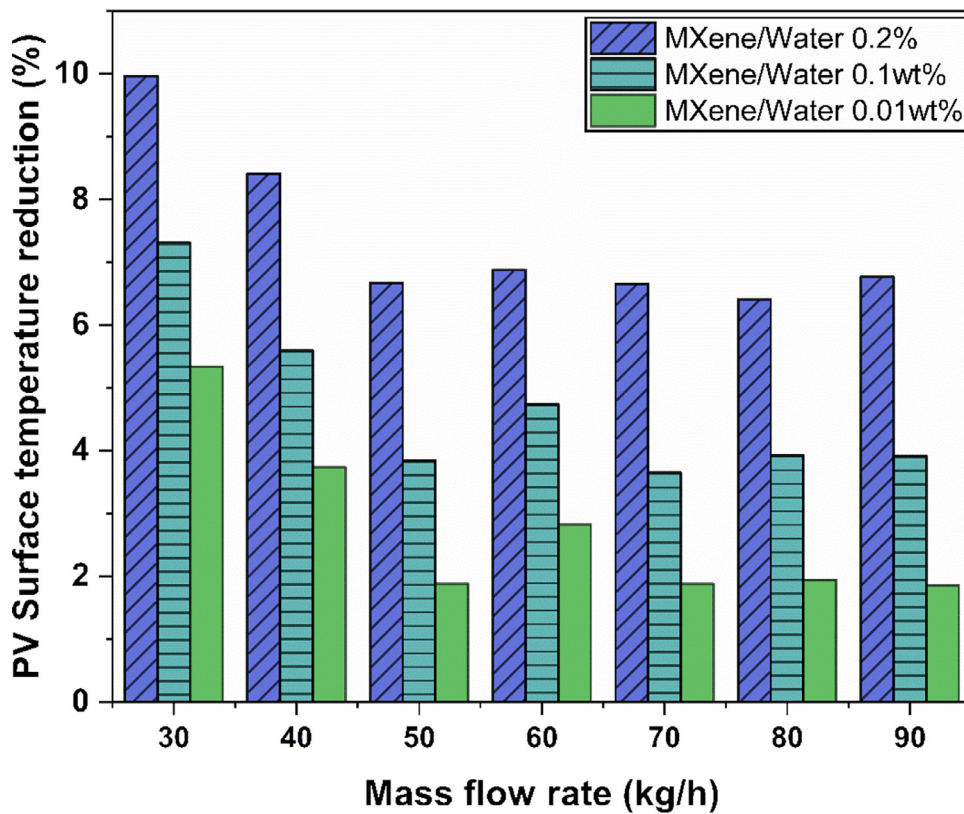
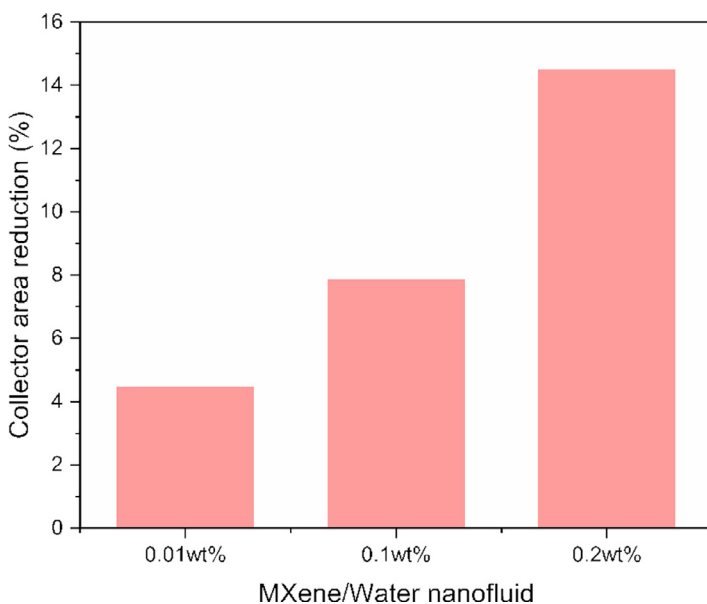


Fig. 13. Effect of nanofluid mass flow rate on PV surface temperature reduction.

**Table 3**  
Nanofluid and base fluid flow property calculation.

Flow rate	Reynolds number ( $Re = \frac{\rho V D}{\mu}$ )				Thermal diffusivity ( $\alpha = \frac{k}{\rho C_p} \cdot 10^{-7} m^2 s^{-1}$ )			
	Water	0.01 wt%	0.1 wt%	0.2 wt%	Water	0.01 wt%	0.1 wt%	0.2 wt%
30	237.84	195.04	71.51	28.68	1.44	1.48	1.90	2.47
40	317.12	260.05	95.35	38.24				
50	396.40	325.07	119.18	47.80				
60	475.68	390.08	143.02	57.36				
70	554.96	455.09	166.86	66.92				
80	634.24	520.11	190.70	76.48				
90	713.52	585.12	214.53	86.04				



**Fig. 14.** Area reduction of PV/T system with nanofluid.

temperature was noticed with the usage of 0.2 wt% of MXene nanofluid over water-based application. The highest reduction could be attributed to the increased thermal property of the nanofluid with higher nanoparticle dispersion (of about 0.2 wt%). However, surface temperature reduction efficiency was found to be decreasing with an increase in flow rate for all the nanofluids. This indicates that even though the PV surface temperature is higher with water compared to nanofluid, the rate of reduction with increasing mass flow rate is high.

### 3.2. Optimization and enviro-economic study

#### 3.2.1. System optimization

The highest thermal efficiencies achieved by water (57.70%), 0.01 wt% (60.40%), 0.1 wt% (62.62%), and 0.2 wt% MXene (67.49%) were selected for analysing the maximum system size reduction possible with nanofluid. Maximum energy efficiency was reported for the highest fluid flow rate of 90  $kg h^{-1}$ . The thermal efficiency achieved by the PV/T system with nanofluids was directly substituted in Eq. (24) to find the equivalent size of PV/T,  $A_{nf}$  ( $m^2$ ), needed to generate the same temperature difference at the same mass flow rate as that of a water-based system. Percentage size reduction of PV/T area ( $A_{red}$ ) achieved by nanofluid over its base fluid (water) was calculated using Eq. (25).

$$A_{nf} = \frac{\dot{m}_{nf} \cdot C_p (T_{out} - T_{in})}{I \eta_{th}} \quad (24)$$

$$A_{red} (\%) = \frac{A_{nf} - A_{water}}{A_{water}} \times 100 \quad (25)$$

For the same thermal output from PV/T, the MXene nanofluid based system achieved a reduction in the collector area by about 4.5 – 14.5%

over a water-based system. The highest size reduction (14.5%) was found to be possible with the 0.2 wt% MXene nanofluid. Corresponding size reduction of the system achieved with 0.1 wt% and 0.01 wt% was calculated to be 7.8% and 4.45%, respectively, as shown in Fig. 14.

#### 3.2.2. Environmental and economic analysis of MXene/water-based PV/T

Energy and exergy performance data of the system was used to assess the environmental, enviro-economic, exergoenvironmental, and exergoenvironmental benefits of using MXene based PV/T. The methodology by Vahidinia et al. (2021) was used for enviroeconomic analysis of the present system. Parameters and their values used in the calculations are shown in Table 4. The amount of carbon dioxide emitted during the working of the PV/T system was calculated using Eq. (26). The corresponding cost associated with the carbon dioxide emission is calculated using Eq. (27) (Vahidinia et al., 2021). The carbon emission cost and the emission rate of PV/T were selected based on data available from the literature.

$$x_{CO_2} = y_{CO_2} Q_{sol} t_{working} \quad (26)$$

$$C_{CO_2} = x_{CO_2} c_{CO_2, PV/T} \quad (27)$$

The  $Q_{sol}$  represents the incident solar energy required by the collector operating with MXene nanofluid for achieving the same energy efficiency as the base fluid. The base fluid that generates comparatively lower overall efficiency for the system was selected as the reference to show the performance enhancement with other working fluid-based PV/T. The overall energy efficiency of EG based PV/T, at base conditions was used in the analysis. The term  $c_{CO_2, PV/T}$  in Eq. (27), indicates the energy-based emission cost ( $\$/kg$  of  $CO_2$ ) for PV/T. The exergoenvironmental analysis of the system is conducted using Eq. (28). While

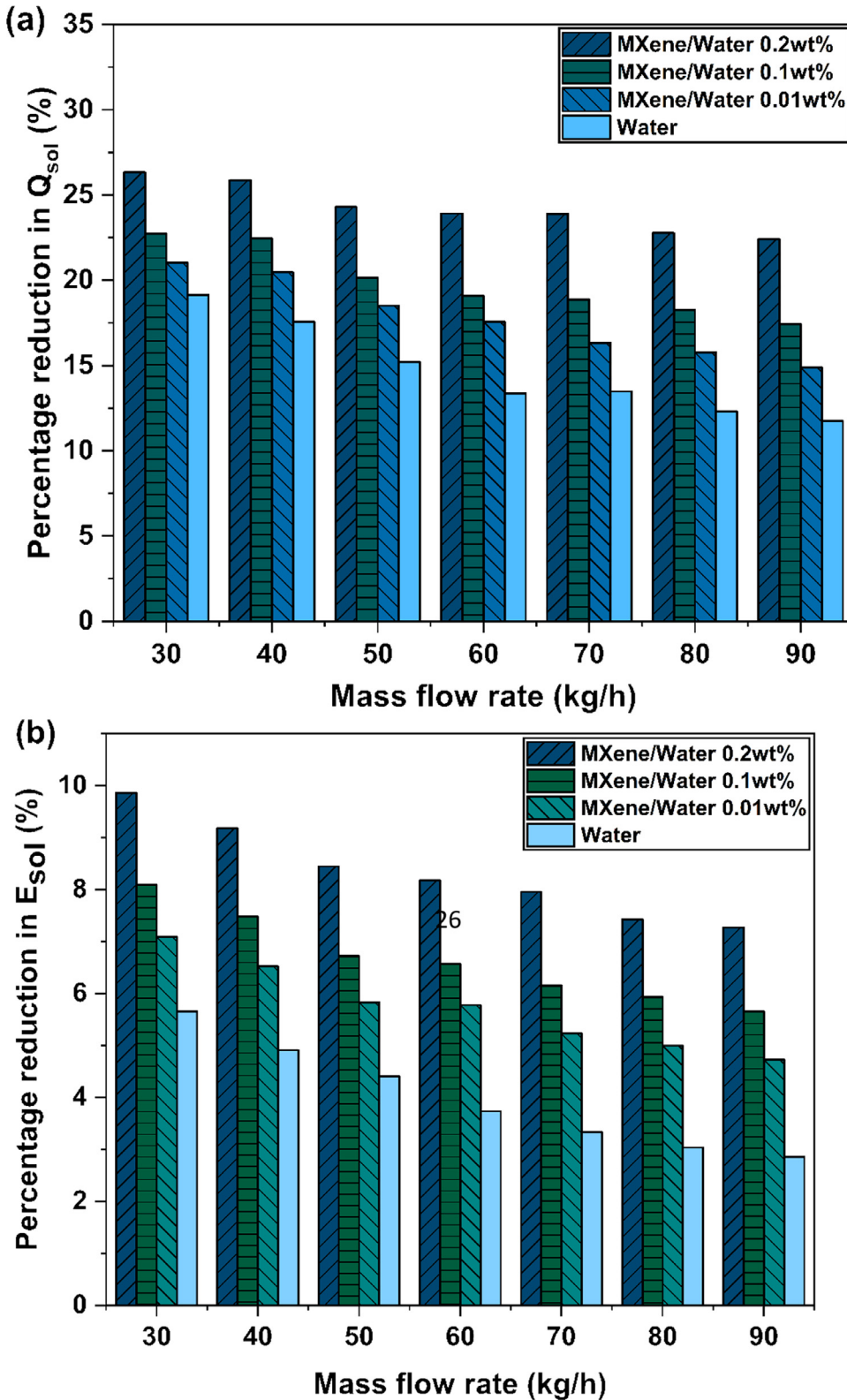


Fig. 15. Percentage reduction of (a) incident solar radiation ( $Q_{sol}$ ), and (b) solar exergy input ( $E_{sol}$ ) for PV/T working on MXene nanofluid and water.

exergoenvironmental analysis is conducted to evaluate the cost associated with the carbon dioxide emission. This analysis based on exergy efficiency of the system is performed using Eq. (29).

$$x_{ex,CO_2} = y_{CO_2} E_{ex, sol}^{working} \tag{28}$$

$$C_{ex,CO_2} = x_{ex,CO_2} c_{CO_2, PV/T} \tag{29}$$

In Eq. (28), the exergy input to the system ( $E_{ex, sol}$ ) is calculated using Eq. (19). For achieving the same exergy efficiency, the solar exergy input required for MXene nanofluid is much less compared to water and EG as shown in Fig. 15 (a). Other operating parameters including incident solar radiation, inlet temperature, and ambient temperatures were kept constant, and the values are provided in Table 4. The

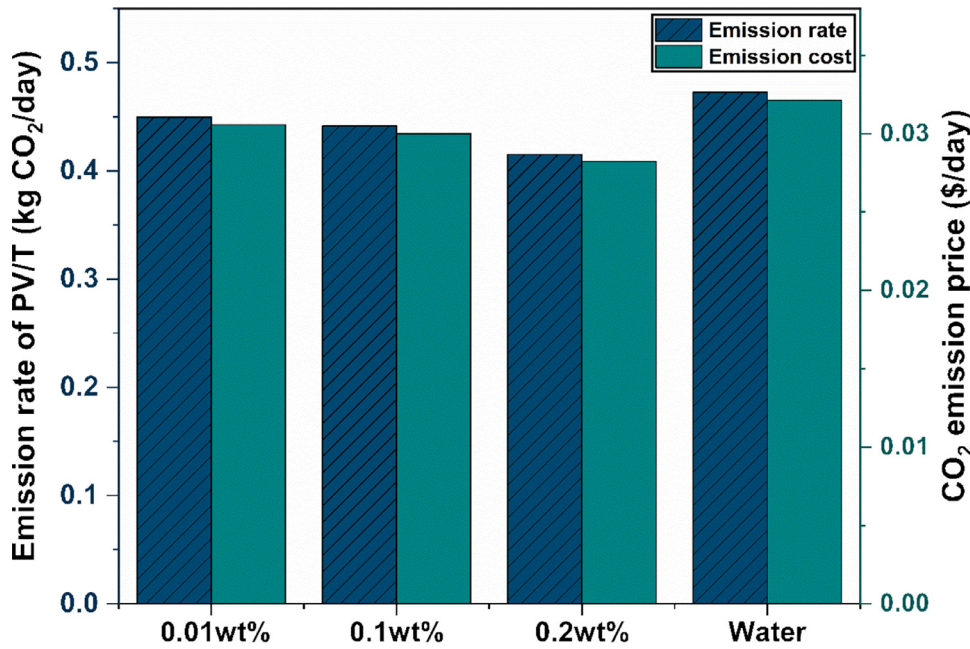


Fig. 16. Energy-based analysis of emission rate (kg CO<sub>2</sub>/day) and emission price (\$/day) of PV/T system operating with nanofluids and water.

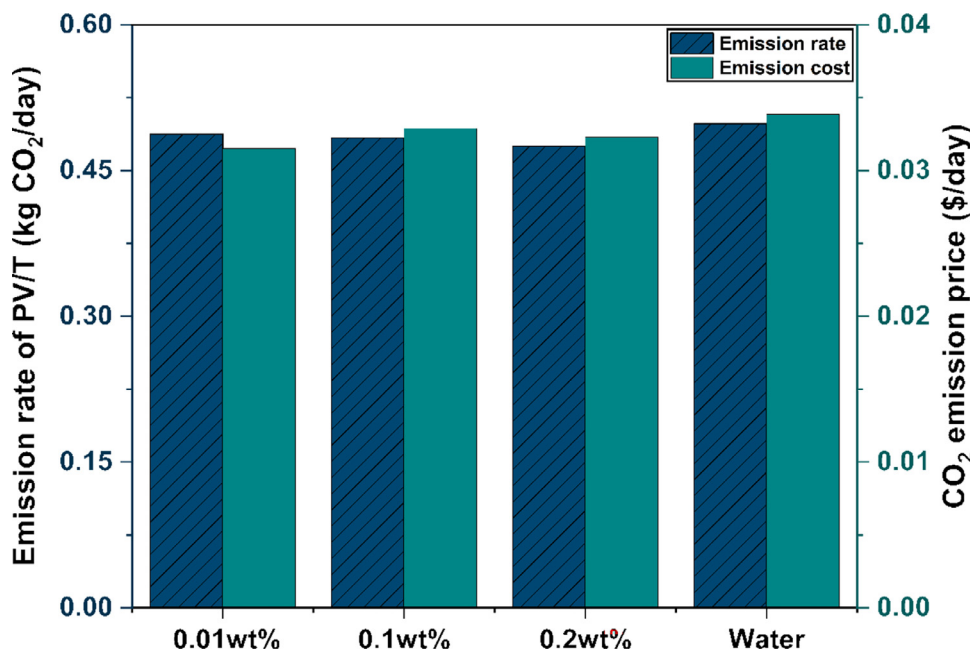


Fig. 17. Exergy based analysis on emission rate (kg CO<sub>2</sub>/day) and emission price (\$/day) of PV/T system operating with nanofluids and water.

Table 4  
Parameters and values used for enviro-economic analysis.

Reference	Parameter	Symbol	Values
Caliskan, 2017	Working hours of PV/T	$t_{working}$	7 h/day
Chow and Ji (2012)	CO <sub>2</sub> emission by PV/T	$y_{CO_2}$	0.000297 kg CO <sub>2</sub> /Wh
Wang et al. (2020)	Energy-based emission cost of PV/T (valid for Hong Kong)	$c_{CO_2, PV/T}$	0.068 \$/kg CO <sub>2</sub>
	Incident solar radiation	-	800 Wm <sup>-2</sup>
	Inlet temperature	-	298 K
	Ambient temperature	-	298 K
	Incident solar energy	$Q_{sol}$	W
	Exergy input to the system	$E_{ex, sol}$	W
	Energy-based daily carbon dioxide emission of PV/T	$x_{CO_2}$	kg CO <sub>2</sub> /day
	Exergy based daily carbon dioxide emission of PV/T	$x_{ex, CO_2}$	kg CO <sub>2</sub> /day
	Energy-based daily emission cost	$C_{CO_2}$	\$/day
	Exergy based daily emission cost	$C_{ex, CO_2}$	\$/day

percentage reduction in  $Q_{sol}$  by working fluids at different flow rates is shown in Fig. 15 (a). The graph shows that 0.2 wt% nanofluid obtained the highest reduction in required energy and exergy by 26.3% and 9.86% respectively, compared to the reference fluid. The daily  $CO_2$  emission rate and emission price for the PV/T system based on the energy perspective are visualized in Fig. 16. As interpreted, the daily  $CO_2$  emission rate was higher for water (0.47  $kgCO_2/day$ ), and lowest for 0.2 wt% MXene (0.42  $kgCO_2/day$ ). The emission rate decreased with nanofluid concentration. The energy-based cost of emission during the working of the system is 0.028224 \$/day for the nanofluid (0.2 wt%). Fig. 17 visualizes the daily emission rate and associated cost based on exergoenvironmental and exergoeconomic analysis. The amount of emission from the system based on exergy analysis using water, and MXene (0.2 wt%) is 0.50, and 0.48  $kgCO_2/day$  respectively. As inferred, 0.2 wt% is reportedly exhibiting a reduced emission rate compared to base fluid and lower concentrations. The cost of emission amounted to 0.034 and 0.032 \$/day for water and 0.2 wt% nanofluid, respectively. Surmising the results, the exergy and energy-based analysis on emission rate and cost of PV/T are almost similar with an average variation of about 8.5%.

#### 4. Conclusions

Numerical modelling of the N-PV/T system was conducted in ANSYS Fluent®. The model was validated with experimental and numerical data in the literature with a minimal error of about 2.75% and 8.9%, respectively. A preliminary study on the heat transfer performance, pressure drop enhancement, thermal efficiency, and electrical efficiency of PV/T with base fluids (water and EG) and MXene nanofluid was conducted at different mass flow rates. Environmental and enviroeconomic assessment was conducted on the system from both energy and exergy perspectives. Major findings from the numerical study and enviroeconomic analysis conducted on MXene based N-PV/T are explained below:

- Ø Numerical CFD simulation shows that thermal and electrical output/efficiency of the system increased with MXene nanofluid mass fraction and flow rate. In the case of 0.2% nanofluid, an increase in the flow rate by 60  $kg\ h^{-1}$  produced a considerable improvement in the thermal efficiency of the system by about 21%. However, the corresponding increase in electrical efficiency of N-PV/T was only about 0.65%.
- Ø The maximum percentage enhancement in thermal efficiency reported by MXene nanofluids of 0.01, 0.1, and 0.2 wt% over the water was about 4.6, 8.5, and 17%, respectively. While the same nanofluids exhibited a percentage enhancement in electrical efficiency by 1.9, 2.6, and 3.5% over water.
- Ø The highest overall energy efficiency attained by N-PV/T with 0.01, 0.1, and 0.2 wt% MXene nanofluid was calculated to be around 76, 78, and 83% at 90  $kg\ h^{-1}$ . Also, the outlet temperature was found to decrease with the flow rate. Even though the pressure drop for nanofluid increased by 88% over water, the pumping power required is considerably small, and significant heat transfer improvement was achieved. For practical implementation of N-PV/T additional cost would be incurred on setting a secondary heat exchanger, long-term stability maintenance steps, and safe disposal. Hence, the proposed efficiency enhancement of the N-PV/T needs to compensate for the additional expenses compared to conventional PV/T.
- Ø Another limitation of the proposed numerical model is the inability to define the stability of nanofluid. This would be addressed in future studies, by incorporating thermophysical characterization data of nanofluid obtained experimentally, for the numerical simulation.
- Ø The feasibility study suggests that for achieving the same thermal efficiency, MXene nanofluid application could reduce the system size by 14.5%.
- Ø Based on overall energy efficiency, the daily  $CO_2$  emission rate and emission cost for the system were the least (0.42  $kgCO_2/day$ ,

and 0.028 \$/day) with 0.2 wt% nanofluid. Similarly, the exergy-based analysis shows that the emission rate of the same fluid is 0.48  $kgCO_2/day$ , and the cost is 0.032 \$/day. However, an increase in the concentration of nanofluid increases the cost of material required per volume of fluid. A detailed economic analysis incorporating the cost for nanomaterial, synthesis method, nanofluid's stability enhancement cost, disposal cost and systems payback period, is necessary to arrive at the cost-effective nanofluid concentration required for N-PVTs and would be conducted in future research work.

#### Declaration of Competing Interest

The authors declare that they have no known competing financial interests or personal relationships that could have appeared to influence the work reported in this paper.

#### Acknowledgement

The authors would like to thank Ulster University for supporting this research through PhD studentship funding from Northern Ireland Department for the Economy. And the authors would like to acknowledge Built Environment Research Institute for the financial support provided for the study. The lab facility provided by Nanotechnology and Integrated Bio-engineering Centre (NIBEC), Ulster University, is also sincerely acknowledged.

#### References

- Ahmadi, A., Ehyaei, M.A., Doustgani, A., El Haj Assad, M., Hmdia, A., Jamali, D.H., Kumar, R., Li, Z.X., Razmjoo, A., 2021. Recent residential applications of low-temperature solar collector. *J. Clean. Prod.* 279. doi:10.1016/j.jclepro.2020.123549.
- ANSYS Inc, 2020. ANSYS FLUENT® Theory Guide Release 2020 R2.
- Arslan, E., Aktaş, M., Can, Ö.F., 2020. Experimental and numerical investigation of a novel photovoltaic thermal (PV/T) collector with the energy and exergy analysis. *J. Clean. Prod.* 276. doi:10.1016/j.jclepro.2020.123255.
- Aste, N., Del Pero, C., Leonforte, F., 2012. Thermal-electrical optimization of the configuration a liquid PVT collector. *Energy Procedia* 30, 1–7. doi:10.1016/j.egypro.2012.11.002.
- Bao, Z., Bing, N., Zhu, X., Xie, H., Yu, W., 2021. Ti3C2Tx MXene contained nanofluids with high thermal conductivity, super colloidal stability and low viscosity. *Chem. Eng. J.* 406, 126390. doi:10.1016/j.ccej.2020.126390.
- Caliskan, H., 2017. Energy, exergy, environmental, enviroeconomic, exergoenvironmental (EXEN) and exergoeconomic (EXENEC) analyses of solar collectors. *Renew. Sustain. Energy Rev.* 69, 488–492. doi:10.1016/j.rser.2016.11.203.
- Chow, T.T., Ji, J., 2012. Environmental life-cycle analysis of hybrid solar photovoltaic/thermal systems for use in Hong Kong. *Int. J. Photoenergy* 2012. doi:10.1155/2012/101968.
- Eisapour, M., Eisapour, A.H., Hosseini, M.J., Talebizadehsardari, P., 2020. Exergy and energy analysis of wavy tubes photovoltaic-thermal systems using microencapsulated PCM nano-slurry coolant fluid. *Appl. Energy* 266, 114849. doi:10.1016/j.apenergy.2020.114849.
- Ekiciler, R., Arslan, K., Turgut, O., Kurşun, B., 2020. Effect of hybrid nanofluid on heat transfer performance of parabolic trough solar collector receiver. *J. Therm. Anal. Calorim.* 143, 1637–1654. doi:10.1007/s10973-020-09717-5.
- Fouad, M.M., Shihata, L.A., Morgan, E.S.I., 2017. An integrated review of factors influencing the performance of photovoltaic panels. *Renew. Sustain. Energy Rev.* 80, 1499–1511. doi:10.1016/j.rser.2017.05.141.
- Green, M.A., Dunlop, E.D., Hohl-Ebinger, J., Yoshita, M., Kopidakis, N., Ho-Baillie, A.W.Y., 2020. Solar cell efficiency tables (Version 55). *Prog. Photovoltaics Res. Appl.* 28, 3–15. doi:10.1002/ppp.3228.
- Gupta, M., Singh, V., Said, Z., 2020. Heat transfer analysis using zinc Ferrite/water (Hybrid) nanofluids in a circular tube: An experimental investigation and development of new correlations for thermophysical and heat transfer properties. *Sustain. Energy Technol. Assessments* 39, 100720. doi:10.1016/j.seta.2020.100720.
- Hussien, A.A., Abdullah, M.Z., Yusop, N.M., Al-Nimr, M.A., Atieh, M.A., Mehrali, M., 2017. Experiment on forced convective heat transfer enhancement using MWCNTs/GNPs hybrid nanofluid and mini-tube. *Int. J. Heat Mass Transf.* 115, 1121–1131. doi:10.1016/j.ijheatmasstransfer.2017.08.120.
- Kandael, A.W., Thakur, A.K., Elkadeem, M.R., Elmorshedy, M.F., Ullah, Z., Sathya-murthy, R., Sharshir, S.W., 2020. Photovoltaics performance improvement using different cooling methodologies: a state-of-art review. *J. Clean. Prod.* 273, 122772. doi:10.1016/j.jclepro.2020.122772.
- Kanti, P.K., Sharma, K.V., Minea, A.A., Kesti, V., 2021. Experimental and computational determination of heat transfer, entropy generation and pressure drop under turbulent flow in a tube with fly ash-Cu hybrid nanofluid. *Int. J. Therm. Sci.* 167, 107016. doi:10.1016/j.ijthermalsci.2021.107016.
- Karaaslan, I., Menlik, T., 2021. Numerical study of a photovoltaic thermal (PV/T) system using mono and hybrid nanofluid. *Sol. Energy* 224, 1260–1270. doi:10.1016/j.solener.2021.06.072.

- Kazemian, A., basati, Y., Khatibi, M., Ma, T., 2021a. Performance prediction and optimization of a photovoltaic thermal system integrated with phase change material using response surface method. *J. Clean. Prod.* 290, 125748. doi:10.1016/j.jclepro.2020.125748.
- Kazemian, A., Parcheforosh, A., Salari, A., Ma, T., 2021b. Optimization of a novel photovoltaic thermal module in series with a solar collector using Taguchi based grey relational analysis. *Sol. Energy* 215, 492–507. doi:10.1016/j.solener.2021.01.006.
- Khanjari, Y., Kasaeian, A.B., Pourfayaz, F., 2017. Evaluating the environmental parameters affecting the performance of photovoltaic thermal system using nanofluid. *Appl. Therm. Eng.* 115, 178–187. doi:10.1016/j.applthermaleng.2016.12.104.
- Khanjari, Y., Pourfayaz, F., Kasaeian, A.B., 2016. Numerical investigation on using of nanofluid in a water-cooled photovoltaic thermal system. *Energy Convers. Manag.* 122, 263–278. doi:10.1016/j.enconman.2016.05.083.
- Kianifard, S., Zamen, M., Nejad, A.A., 2020. Modeling, designing and fabrication of a novel PV/T cooling system using half pipe. *J. Clean. Prod.* 253, 119972. doi:10.1016/j.jclepro.2020.119972.
- Mahesh, K.V., Linsha, V., Peer Mohamed, A., Ananthakumar, S., 2016. Processing of 2D-MAXene nanostructures and design of high thermal conducting, rheo-controlled MAXene nanofluids as a potential nanocoolant. *Chem. Eng. J.* 297, 158–169. doi:10.1016/j.cej.2016.04.010.
- Mashhadian, A., Mahdi, M., Mahian, O., 2021. Improving environmental performance of a direct absorption parabolic trough collector by using hybrid nanofluids 244.
- Nasrin, R., Rahim, N.A., Fayaz, H., Hasanuzzaman, M., 2018. Water/MWCNT nanofluid based cooling system of PVT: Experimental and numerical research. *Renew. Energy* 121, 286–300. doi:10.1016/j.renene.2018.01.014.
- Parashar, N., Aslfattahi, N., Yahya, S.M., Saidur, R., 2021. ANN modeling of thermal conductivity and viscosity of MXene-based aqueous ionanofluid. *Int. J. Thermophys.* 42, 1–24. doi:10.1007/s10765-020-02779-5.
- Pordanjani, A.H., Aghakhani, S., Afrand, M., Sharifpur, M., Meyer, J.P., Xu, H., Ali, H.M., Karimi, N., Cheraghian, G., 2021. Nanofluids: Physical phenomena, applications in thermal systems and the environment effects- a critical review. *J. Clean. Prod.* 320, 128573. doi:10.1016/j.jclepro.2021.128573.
- Radwan, A., Katsura, T., Memon, S., Abo-Zahhad, E.M., Abdelrehim, O., Serageldin, A.A., Elmarghany, M.R., Khater, A., Nagano, K., 2020. Development of a new vacuum-based photovoltaic/thermal collector, and its thermal and exergy analyses. *Sustain. Energy Fuels* 4, 6251–6273. doi:10.1039/d0se01102a.
- Rejeb, O., Sardarabadi, M., Ménéz, C., Passandideh-Fard, M., Dhaou, M.H., Jemni, A., 2016. Numerical and model validation of uncovered nanofluid sheet and tube type photovoltaic thermal solar system. *Energy Convers. Manag.* 110, 367–377. doi:10.1016/j.enconman.2015.11.063.
- Rubbi, F., Habib, K., Saidur, R., Aslfattahi, N., Yahya, S.M., Das, L., 2020. Performance optimization of a hybrid PV/T solar system using Soybean oil/MXene nanofluids as A new class of heat transfer fluids. *Sol. Energy* 208, 124–138. doi:10.1016/j.solener.2020.07.060.
- Salameh, T., Tawalbeh, M., Juaidi, A., Abdallah, R., Hamid, A., 2021. A novel three-dimensional numerical model for PV /T water system in hot climate region. *Renew. Energy* 164, 1320–1333. doi:10.1016/j.renene.2020.10.137.
- Salari, A., Taheri, A., Farzanehnia, A., Passandideh-fard, M., Sardarabadi, M., 2020. An updated review of the performance of nanofluid-based photovoltaic thermal systems from energy, exergy, economic, and environmental (4E) approaches. *J. Clean. Prod.* 124318. doi:10.1016/j.jclepro.2020.124318.
- Samyalingam, L., Aslfattahi, N., Saidur, R., Yahya, S.M., Afzal, A., Arifutzzaman, A., Tan, K.H., Kadirgama, K., 2020. Thermal and energy performance improvement of hybrid PV/T system by using olein palm oil with MXene as a new class of heat transfer fluid. *Sol. Energy Mater. Sol. Cells* 218, 110754. doi:10.1016/j.solmat.2020.110754.
- Sangeetha, M., Manigandan, S., Chaichan, M.T., Kumar, V., 2020. Progress of MWCNT, Al<sub>2</sub>O<sub>3</sub>, and CuO with water in enhancing the photovoltaic thermal system. *Int. J. Energy Res.* 44, 821–832. doi:10.1002/er.4905.
- Selmi, M., Al-Khawaja, M.J., Marafia, A., 2008. Validation of CFD simulation for flat plate solar energy collector. *Renew. Energy* 33, 383–387. doi:10.1016/j.renene.2007.02.003.
- Shahsavari, A., 2021. Experimental evaluation of energy and exergy performance of a nanofluid-based photovoltaic/thermal system equipped with a sheet-and-sinusoidal serpentine tube collector. *J. Clean. Prod.* 287, 125064. doi:10.1016/j.jclepro.2020.125064.
- Sreedhar, T., Nageswara Rao, B., Vinay Kumar, D., 2020. Heat transfer enhancement with different nanofluids in heat exchanger by CFD. *Lect. Notes Mech. Eng.* 387–397. doi:10.1007/978-981-32-9931-3\_38.
- Sreekumar, S., Joseph, A., Sujith Kumar, C.S., Thomas, S., 2020. Investigation on influence of antimony tin oxide/silver nanofluid on direct absorption parabolic solar collector. *J. Clean. Prod.* 249, 119378. doi:10.1016/j.jclepro.2019.119378.
- Sreekumar, S., Shah, N., Mondol, J., Hewitt, N., Chakrabarti, S., 2022. Broadband absorbing mono, blended and hybrid nanofluids for direct absorption solar collector: a comprehensive review. *Nano. Futur.* doi:10.1088/2399-1984/ac57f7.
- Vahidinia, F., Khorasanizadeh, H., Aghaei, A., 2021. Comparative energy, exergy and CO<sub>2</sub> emission evaluations of a LS-2 parabolic trough solar collector using Al<sub>2</sub>O<sub>3</sub>/SiO<sub>2</sub>-Syltherm 800 hybrid nanofluid. *Energy Convers. Manag.* 245, 114596. doi:10.1016/j.enconman.2021.114596.
- Wahab, A., Khan, M.A.Z., Hassan, A., 2020. Impact of graphene nanofluid and phase change material on hybrid photovoltaic thermal system: exergy analysis. *J. Clean. Prod.* 277, 123370. doi:10.1016/j.jclepro.2020.123370.
- Wang, Y., Winchester, N., Webster, C.J., Nam, K.M., 2020. Impacts of China's emissions trading scheme on the national and hong kong economies: a dynamic computable general equilibrium analysis. *Front. Environ. Sci.* 8, 1–15. doi:10.3389/fenvs.2020.599231.